NASA Technical Memorandum 83579

Real-Time Hybrid Computer Simulation of a Small Turboshaft Engine and Control System

Clint E. Hart and Leon M. Wenzel
Lewis Research Center
Cleveland, Ohio

February 1984

NASA

REAL-TIME HYBRID COMPUTER SIMULATION OF A SMALL TURBOSHAFT ENGINE AND CONTROL SYSTEM

Clint E. Hart and Leon M. Wenzel

National Aeronautics and Space Administration
Lewis Research Center
Cleveland, Ohio 44135

SUMMARY

This report describes the development of an analytical model of a small turboshaft engine designed for helicopter propulsion systems. The model equations were implemented on a hybrid computer system to provide a real-time nonlinear simulation of the engine performance over a wide operating range. The real-time hybrid simulation of the engine was used as a test bed for evaluating a microprocessor-based digital control module. This digital control module was developed as part of an advanced rotorcraft control program that has the long-term goal of rotorcraft flight and propulsion control integration. After tests with the hybrid engine simulation the digital control module was used to control a real engine in an experimental program.

A hybrid simulation of the engine's electrical-hydromechanical control system was also developed. This provided a convenient way of varying the fuel flow and torque load inputs to the hybrid engine simulation for simulating transient operation. A comparison of steady-state data obtained from the simulation and the experimental tests is presented that validates the simulation results. Analytical model equations, analog computer diagrams, and a digital computer flow chart are given in the appendixes.

INTRODUCTION

New mission requirements for helicopters are leading to demands for faster response from the helicopter propulsion system and its associated control. The most common helicopter propulsion system employs one or two small turboshaft engines. Current turboshaft engine controls use pneumatic, hydraulic, and mechanical components to perform the control sensing, computation, and actuation. There are limitations on the dynamic response of these types of component and the complexity of the control functions that they can handle. One means of overcoming these limitations is to use digital electronic components to implement the control and logic functions in the control system. Digital control systems have proved to be feasible for other complex gas turbine control applications (refs. 1 and 2).

The design of helicopter propulsion controls is complicated by the very close dynamic coupling between the airframe and the propulsion system. Dynamic interaction between the fuel control system and the flexible rotor and drivetrain has been minimized by making the fuel control very slow. Advanced, integrated controls are required to allow faster engine response while avoiding adverse coupling between engine and airframe. This will allow tighter rotor speed control and will reduce pilot workload.

In developing helicopter engines and their control systems there are usually several iterations before the design is finalized. This build-and-test cycle can be very costly and time consuming, especially if major changes must be made to the control system hardware. Therefore, better analytical tools are needed by the control system designers. Computer simulations of gas turbine engines have proved to be a valuable aid in the control design process (ref. 3). In particular, real-time engine simulations are a cost-effective way of evaluating and validating digital control hardware and software prior to full-scale engine testing (ref. 4).

A program is now under way at the NASA Lewis Research Center to develop and evaluate advanced control modes for small turboshaft engines. An initial task of this program was to design and build a microprocessor-based digital control module that could be programmed to perform the control and logic functions for the engine control system. This digital control module replaces the original control system hardware and performs all of the engine control functions except fuel metering and actuation of the fuel-metering valve and compressor variable geometry. For experimental engine tests the digital control module provides electrical signals to a modified hydromechanical unit (HMU) that performs the fuel metering and variable-geometry control.

Initially the digital control module was programmed to duplicate the control and logic functions of the original control system. To evaluate this digital control implementation, before actual engine testing, a real-time hybrid computer simulation of the small turboshaft engine was developed. This engine simulation provided realistic inputs to the digital control module over the normal operating range. After the digital control implementation was validated, the digital control module was used to control an actual engine. Later in the program, advanced control modes will be programmed on the digital control module and evaluated by using the real-time engine simulation prior to engine tests.

To aid in validating the steady-state and transient performance of the engine simulation, a real-time hybrid computer simulation of the original control system was developed. This provided a convenient way of varying the engine set point and facilitated running transients to assess engine simulation dynamics. This report documents the hybrid computer simulations of the engine and control system and the procedures used in developing them.

In the following sections the engine and the control system are described. The mathematical modeling of engine component performance and how this was implemented on a hybrid computer are then discussed. The simulation of the original engine control system on the hybrid computer is also discussed. Finally, results are presented from comparisons of experimental and simulation steady-state data. The appendixes contain lists of equations for the engine and control simulation models. Detailed analog diagrams and a flow chart for the digital function generation program are also included in the appendixes.

ENGINE DESCRIPTION

The engine selected for this simulation is a small, lightweight turboshaft engine of the 1500-horsepower class (fig. 1). It has a five-axial-stage, single-centrifugal-stage compressor with variable inlet guide vanes and variable stator vanes for the first two stages. The combustor is annular with

central fuel injectors and vortex air swirlers. The gas generator turbine that drives the compressor rotor is a two-stage, air-cooled, axial design. Air is bled from the compressor exit to cool this turbine. The two-stage power turbine is uncooled. It has a coaxial driveshaft that extends forward through the gas generator and connects through a splined joint to the engine output shaft.

DEVELOPMENT OF ENGINE MODEL

In developing the computer simulation of the small turboshaft engine, each of the major components (e.g., compressor, combustor, and turbine) was modeled by functions representing its steady-state performance data (maps) or a set of algebraic equations. The total volume associated with the flow passages in the engine was distributed among a number of mixing volumes that connected the individual component models. Angular momentum equations represent the differential torque-speed relationship of the two rotating shafts. These shafts connect the compressor and gas generator turbine models and the power turbine and load (rotor) models.

A block diagram of the small turboshaft engine is shown in figure 2. The principal engine variables - pressures, temperatures, flows, torques, and rotational speeds - are shown on the diagram. The numbers are engine station designations. This block diagram can be viewed as a computational flow diagram. Each engine variable is represented by a line with a directional arrow to indicate the flow of information from one component model to another. The input-output relationships for a particular component are governed by thermodynamic or aerodynamic processes. These relationships are represented mathematically by differential equations, algebraic equations, or single or multivariable functions.

Most simulations have special requirements that depend on their application. For a computer simulation that is to be used for hardware-in-the-loop control system studies, one requirement is that it compute both the steady-state values and transient response of the principal engine variables over the operating range of interest. A second requirement is that it compute engine variables on a real-time basis. The latter requirement is to allow interfacing with the control system hardware, which operates in real time.

After drawing the computational flow diagram the next step was to obtain steady-state values of the engine variables over the desired operating range. There were two sources of these data. The primary source was the manufacturer's engine performance computer program, which was developed during the engine design phase. The second source was engine experimental test data. For the small turboshaft engine simulation development the performance program was used to obtain steady-state values of the engine variables for 60 operating points. Each operating point was defined by a value of power turbine speed (85 to 105 percent of design speed) and a value of power output (6.67 to 100 percent of design power). All operating points that were selected corresponded to sea-level static operation.

Mathematical equations (or tabular function data) to represent the input-output relationships for each engine component were determined from these steady-state data. The basic equations, their derivations, and the forms of the functions have been presented in many engine simulation reports (e.g.,

refs. 5 to 7). For the small turboshaft engine some of the basic equations and functions were simplified.

The equations and functions were first programmed in the Continuous System Modeling Program (CSMP) simulation language and run in nonreal time on the IBM 370/3033 mainframe computer. The purpose was to determine if a simplified set of equations and functions could adequately represent the steady-state performance of the engine. Several simplifications were considered, check cases were run, and steady-state results were compared with results from the more detailed performance program. A final model was selected that computed key engine variables within 1 percent of the performance program values.

The next step was to compare the results from the CSMP program with available experimental test data. However, two problems were encountered. First, the engine used for the experimental tests was a nonstandard design containing modified compressor and turbine components. Thus the data used to develop the CSMP model did not represent the modified engine. Second, the experimental test data were insufficient to completely define the engine model. Only 12 engine variables were measured. These included a total engine airflow "measurement" that was actually calculated from pressure and temperature measurements upstream of the engine. No measurements of pressures or temperatures were made in the hot section of the engine except for the interturbine temperature (station 45) and the exit pressure and temperature (station 49).

To develop a CSMP model that could duplicate the experimental engine test data, a more complete set of engine data had to be constructed. A procedure for synthesizing missing engine data had been developed as an application of data analysis software written for a small digital computer (ref. 8). The synthesis procedure was based on energy and flow balance relationships for this type of engine. By using the 12 measured variables, 40 additional engine variables (and combinations thereof) were calculated at each of six test conditions. From this set of calculated and measured engine variables a modified CSMP model of the experimental engine was derived. The equations for the modified CSMP model are given in appendix B. Appendix B also briefly describes the mathematical representation of each component's performance. Symbols are defined in appendix A.

The modified CSMP model, like most other digital simulation models, did not run in real time. However, it did provide certain advantages. For example, changes in the model structure and component performance functions were easily made with CSMP. Also, floating-point data obtained from the CSMP model, over a wide range of operating conditions, provided scaling information needed for the fixed-point hybrid computer simulation.

HYBRID COMPUTER SIMULATION OF ENGINE

The equations and functions for the experimental engine model, given in appendix B, were implemented on one of the Lewis Research Center's two hybrid computing systems. Each system consists of an EAI PACER 100 digital computer and two EAI 681 analog computers plus peripherals. For the engine simulation the digital computer was used for initial setup (i.e., setting coefficient potentiometers and function generators), static operation check (i.e., patching and component checking), and digital function generation for the dual-variable compressor map and one of the single-variable turbine functions. One

of the analog computers was used for all of the other calculations (i.e., summation, integration, multiplication, division, and single-variable function generation). The second analog computer was used to implement the simulation of the original engine control system. The control system simulation is discussed later. Analog-to-digital (A/D) and digital-to-analog (D/A) converters were used to transfer signals between the analog and digital computers. The update time of the digital computer (i.e., A/D conversion, function table lookup and interpolation, and D/A conversion) was less than 4 milliseconds. This allowed the simulation to run in real time. Diagrams for the analog computer part of the hybrid simulation and a flow chart for the digital program are contained in appendix C.

To validate the hybrid computer simulation of the engine, the simulation was run to obtain both steady-state and transient data. Steady-state data were obtained by setting fixed values for inlet pressure P2, inlet temperature T2, outlet pressure P49, fuel flow WF, and load torque TORQLD and letting the computer calculate all other engine variables. However, to obtain transient data it was necessary to provide WF and TORQLD inputs as functions of time. Instead of scheduling these inputs as functions of time for a number of different "real world" transients, a more direct approach was selected. A computer model of the actual engine control hardware was developed to provide the necessary time-varying inputs to the engine simulation in response to changes in the control system inputs. This model also provided information about internal variables in the control system to aid in developing and debugging software for the microprocessor-based digital control module. The engine control system is described in the following section.

CONTROL SYSTEM DESCRIPTION

The engine control system was designed to provide complete and safe control of the engine and to reduce the pilot's workload. Some of the functions it provides are automatic startup, compressor bleed and variable-geometry control, rotor speed control for varying load conditions, and torque matching for multiple-engine installations. It also protects the engine from overspeed, overtemperature, and other unsafe operating conditions.

The engine control system consists of an electrical control unit (ECU) and a hydromechanical control unit (HMU). Basically, the HMU meters fuel flow to the engine as a function of gas generator speed NG, inlet temperature T2, compressor outlet pressure P3, an electrical trim signal from the ECU, plus pilot inputs of power-available spindle angle PAS, and load-demand spindle angle LDS. Rapid engine transient response to load-demand changes is provided by a feed-forward signal from the LDS input. Acceleration limiting, stall and flameout protection, gas generator speed limiting, and variable-geometry actuation are also provided by the HMU.

The ECU provides an electrical trim signal to the HMU to satisfy the load requirements so as to maintain constant rotor speed and load sharing for multiple-engine operation. It also limits power turbine inlet temperature and total delivered torque and provides a separate signal to a fuel-sequencing valve for power turbine overspeed protection.

Detailed information was obtained from the engine manufacturer to develop a model of the engine control system. A block diagram that represents the

principal components of the engine control system is shown in figure 3. The equations, functions, and logic relationships that mathematically represent the performance of these components are given in appendix B. Certain functions of the actual control system were not included in the simulation. These were automatic startup, variable-geometry control, and torque matching for multiple-engine installations.

HYBRID COMPUTER SIMULATION OF CONTROL SYSTEM

The equations, functions, and logic representing the control system model were implemented on the second analog computer of the hybrid computer system. The bivariable functions representing the acceleration schedule and the thermocouple harness time constant were calculated on the digital computer. All other equations and logic were calculated on the analog computer. Analog diagrams and digital flow charts of the control system are included in appendix C.

RESULTS AND DISCUSSION

To determine how well the CSMP and hybrid simulations represent the engine steady-state performance, six test conditions were evaluated. At each test condition, values of inlet pressure P2, inlet temperature T2, outlet pressure P49, fuel flow WF, and load torque TORQLD were determined from experimental data. Table I lists the values for the six selected test conditions. These values were used as inputs to the simulations, which were run until steady-state conditions were reached. For the CSMP simulations all calculated variables were printed out. For the hybrid simulations only the principal engine variables were recorded.

The experimental test values and simulation results for key engine variables are shown in table II. Agreement between simulation and experimental test values is quite good, with a maximum difference of about 3 percent. The largest differences occurred in the hot-section temperatures T45 and T49. Since the digital and hybrid engine simulations were programmed from the same model equations and function data, the observed differences between the digital and hybrid simulation results were attributed to slight inaccuracies in the analog computer components (i.e., function generators, multipliers, and summers).

To check the transient operation, the combined hybrid simulation of the engine and control system was exercised by manipulating the LDS and PAS inputs as would the pilot of a helicopter. Typically the LDS input varies the collective pitch of the helicopter rotor system and thus the torque load on the power turbine shaft. Changing the LDS input also sends to the fuel flow control loop an anticipatory signal that indicates the load is changing.

Rapid linear changes were made in the LDS input between idle and high load demand. Internal variables in the control system as well as principal engine variables were monitored. This provided a check on operation of the selection logic, which modifies the engine control according to various schedules and engine variable limits. The PAS input was also varied to check its effect on engine operation.

Although transient performance data were obtained from the hybrid simulation, no satisfactory transient data were available from experimental engine tests for comparison. However, the transient data from the simulation could be judged qualitatively from the standpoint of reasonableness and did provide helpful scaling information for developing the software for the microprocessor-based digital control module.

Typical transient response of certain engine variables to changes in the LDS input are shown in the strip-chart recording in figure 4. The LDS input was ramped from 60° to 0° in 2 seconds. After a short settling period LDS was ramped back to 60°. The control maintained the power turbine speed NP to within 2 percent of the desired value. The torque reference, which represents the load on the power turbine, is a second-order function of LDS and NP. The scales on the speed traces are percent of design. The scales on the torque, WF, and PS3 traces are percent of full scale. The scale on the T45 trace is percent of the overtemperature limit value.

After the digital control module was programmed, it was connected to the hybrid engine simulation. The LDS input was varied as it was for the transients with the hybrid control simulation. The initial transient data indicated software errors. These errors were found and corrected. Subsequent transient response data, shown in figure 5, closely match those shown in figure 4.

The digital control module was also programmed to provide logic for engine startup, engine overspeed protection, and sensor failure detection. All of these modes of control operation were successfully validated prior to actual engine testing with the aid of the hybrid engine simulation.

CONCLUDING REMARKS

A real-time hybrid computer simulation of a small turboshaft engine and its control system has been developed. For steady-state operation, engine performance data from the simulation compared very well with similar data from actual engine tests. Because of lack of experimental transient data no comparison with the simulation data was possible. However, the simulation is believed to represent real transient performance well enough to be used as a design aid and test bed for developing a digital control module for a small turboshaft engine. The simulation has been used successfully to test new digital control hardware and software. Software errors have been found and corrected before actual engine testing. The simulation has provided valuable insights into the steady-state and transient behavior of the engine and its control and has therefore served as a training tool for the controls engineer.

APPENDIX A

SYMBOLS

Variables and Coefficients Used in Engine Simulation

B1	bleed fraction (function of PCNGC)
B2	bleed fraction (function of WA2C)
DEL2	ratio of total inlet pressure to sea-level pressure
DH	enthalpy drop, J/kg (Btu/lbm)
DHQTH4	enthalpy drop parameter for gas generator turbine, J/kg (Btu/lbm)
DHQTH5	enthalpy drop parameter for power turbine, J/kg (Btu/lbm)
dt	differential time, sec
EFFB	combustor efficiency, fractional percent
FAR	fuel-air ratio
H	enthalpy, J/kg (Btu/lbm)
HVF	heating value of fuel, J/kg (Btu/lbm)
I	polar moment of inertia, $N\text{-}m\text{-}sec^2$ ($ft\text{-}lbf\text{-}sec^2$)
ICX	initial condition of state variable X
KDPB	combustor pressure drop coefficient, $N^2\text{-}sec^2/kg^2\text{-}cm^4\text{-}K$ ($lbf^2\text{-}sec^2/lbm^2\text{-}in^4\text{-}°R$)
KINR	angular velocity conversion coefficient, rpm-sec/radian
KTRQ	torque conversion coefficient, N-m-rpm-sec/J-radian (lbf-ft-rpm-sec/Btu-radian)
KV	volume coefficient, $N/cm^2\text{-}kg\text{-}K$ ($lbf/in^2\text{-}lbm\text{-}°R$)
KW	flow coefficient, $kg\text{-}cm^2/N\text{-}sec$ ($lbm\text{-}in^2/lbf\text{-}sec$)
LDS	load-demand spindle angle, deg
NG	rotational speed of compressor, rpm
NP	rotational speed of power turbine, rpm
P	total pressure, N/cm^2 (psia)
PCNG	rotational speed of compressor, percent of design speed
PR	pressure ratio
PS	static pressure, N/cm^2 (psia)
PS3Q2	pressure ratio (compressor exit static to inlet total)
TH2	ratio of inlet total temperature to standard-day temperature
T	total temperature, K (°R)
TAU	time constant, sec
THTA	squared critical velocity ratio
TORQ	torque, N-m (ft-lbf)

T3Q2	temperature ratio (compressor exit total to inlet total)
W	mass flow rate, kg/sec (lbm/sec)
WS	stored mass, kg (lbm)
WXQ2	bleed coefficient (function of WA2C)

Qualifiers and Station Designations

A	air
B	combustor
BL	bleed air
C	corrected value
CM	compressor
DSN	design value
F	fuel
GT	gas turbine
L	lagged
LD	load
PH	per hour
PT	power turbine
2	compressor inlet
25	intercompressor bleed port
3	compressor outlet
31	combustor inlet
41	gas generator turbine inlet
44	gas generator turbine outlet
45	power turbine inlet
49	power turbine outlet

Variables and Coefficients Used in Control System Simulation

DWFPL	incremental fuel flow demand signal due to LDS
ICX	initial condition of state variable X
KGVNR	NP governor rate compensation gain
KINTG	integral gain (ECU compensation)
KNDRP	NG droop line slope
KNGVN	additional NP governor gain
KNTRM	speed error trim gain (normal), V/rpm

KPROP	proportional gain (ECU compensation)
KSPDS	NP governor gain
KTMC	torque motor coil conductance, mA/V
KTMFB	torque motor LVDT feedback gain, V/cm (V/in.)
KTMLO	torque motor sensitivity, cm/sec-mA (in./sec-mA)
KTMRU	torque motor linkage gain, cm/cm (in./in.)
KTMSR	torque motor compensation gain, V/V
KTSG1	T45 limiter compensation gain
KT45LM	T45 limiter gain
KWFD	midrange slope (deceleration schedule)
KWLDSR	reference level (LDS WF/PS3 demand signal)
PAS	power-available spindle angle, deg
PCNGD	NG demand based on LDS, percent of design speed
PCNGDH	upper NG limit (deceleration schedule), percent of design speed
PCNGLDL	lower NG limit (deceleration schedule), percent of design speed
PCNGI	reference for idle NG droop line (function of T2), percent of design speed
PCNGS	sensed gas generator turbine speed, percent of design speed
PCNPRF	power turbine speed reference, percent of design speed
PCNPS	sensed power turbine speed, percent of design speed
PS3L	sensed PS3, N/cm^2 (psia)
RULDS	fuel flow demand trim signal from LDS and ECU
SPDB	speed error threshold for additional NP governor gain, percent of design speed
SPDER	power turbine speed error, percent of design speed
SPDG	ECU trim demand signal, V
SPDL	speed error with governor rate lag compensation
SPDR	speed error above threshold value, percent of design speed
SPRDC	speed error with rate compensation
SPRD2	speed error with governor rate compensation
SPDS	speed error with governor lag
SPDSF	speed error with governor dynamics
SPDSHL	high limit of integral of speed error
SPDSI	speed error with integral compensation
SPDSIL	integral of speed error (after limiter)
SPDSL	speed error with governor lead-lag
SPDSLL	low limit of integral of speed error

SPDSP	speed error with proportional compensation
SPDSS	selected maximum error (NP or T45 overlimit)
SPDS1	speed error with trim gain and governor rate compensation
SPDS2	speed error with additional gain and governor rate compensation
TCGRLD	time constant (NP governor rate compensation, lead), sec
TCGRLG	time constant (NP governor rate compensation, lag), sec
TCGVLD	time constant (governor loop lead), sec
TCGVLG	time constant (governor loop lag), sec
TCNGS	time constant (NG sensor lag), sec
TCPS3	time constant (PS3 sensor), sec
TCSPDG	time constant (ECU trim signal lag), sec
TCTMSR	time constant (torque motor lag compensation), sec
TC45	time constant (T45 harness lag (fixed)), sec
TC45H	time constant (T45 harness lag (variable)), sec
TC45L	time constant (T45 limiter lag), sec
TC45LD	time constant (T45 limiter lead compensation), sec
TC45LG	time constant (T45 limiter lag compensation), sec
TERR	T45 overtemperature error, K (°R)
TMBS1	torque motor error bias, V
TMBS2	torque motor current bias, mA
TMDB	torque motor current deadband, mA
TMI	torque motor current, mA
TMILIM	torque motor current limit, mA
TMLO	torque motor flapper position, cm (in.)
TMLDL	torque motor flapper position limited, cm (in.)
TMRU	WF/PS3 trim signal
TMSE	torque motor error signal, V
TMSIG	torque motor current (with deadband), mA
TMSL	intermediate torque motor error compensated, V
TMSLL	torque motor error compensated, V
TMSR	torque motor error compensated, V
TSGE	T45 error with lag, K (°R)
TSGL	intermediate T45 error compensated, K (°R)
TSIG	T45 error compensated, K (°R)
TSIGS	T45 positive error signal to selector, K (°R)
T45COR	T45 harness correlation, K (°R)
T45E	T45 plus harness correlation, K (°R)

T45EL	T45 sensed, K (°R)
T45L	T45 sensed intermediate, K (°R)
T45LIM	T45 maximum limit, K (°R)
WF	fuel flow (after limiting), kg/hr (lbm/hr)
WFIDM	WF/PS3 demand limit signal (idle schedule)
WFIRF	WF/PS3 demand value (idle schedule limiting value; function of T2)
WFMAX	maximum fuel flow limit, kg/hr (lbm/hr)
WFMIN	minimum fuel flow limit, kg/hr (lbm/hr)
WFMV	fuel flow (after limiting), kg/hr (lbm/hr)
WFPAC	WF/PS3 demand limit signal (acceleration schedule)
WFPDC	WF/PS3 demand limit signal (deceleration schedule)
WFPDCH	upper limit WF/PS3 demand (deceleration schedule)
WFPDCL	lower limit WF/PS3 demand (deceleration schedule)
WFPDM	combined WF/PS3 demand signal before limits
WFPDRP	ΔWF/PS3 demand signal (droop line)
WFPDO	WF/PS3 demand signal (after idle limit selector)
WFPD1	WF/PS3 demand signal (after acceleration limit selector)
WFPD2	WF/PS3 demand signal (after acceleration limit selector)
WFPRF	ΔWF/PS3 demand signal (function of PAS)
WFPTP	WF/PS3 demand value (topping level)
WFQD	ΔWF/PS3 demand signal (function of LDS)
W45R	power turbine flow parameter, kg-cm^2-K$^{1/2}$/N-sec (lbm-in^2-°R$^{1/2}$/lbf-sec)

APPENDIX B

MATHEMATICAL REPRESENTATION OF ENGINE AND CONTROL COMPONENTS

Engine Components

Compressor. - The corrected compressor airflow is calculated from an overall performance map that is a bivariable function of pressure ratio and corrected rotor speed. The temperature ratio across the compressor is a nonlinear function of pressure ratio. The bleed flow fractions, for compressor interstage bleed, are functions of corrected rotor speed and airflow.

$$PCNGC = NGC/NGDSN * 100 \tag{B1}$$

$$PS3Q2 = PS3/P2 \tag{B2}$$

$$WA2C = f_1\ (PS3Q2, PCNGC) \tag{B3}$$

$$WA2 = WA2C * DEL2/\sqrt{TH2} \tag{B4}$$

$$H2 = 889.5 * T2 \tag{B5}$$

$$T3Q2 = f_2\ (PS3Q2) \tag{B6}$$

$$T3 = T3Q2 * T2 \tag{B7}$$

$$B1 = f_3\ (PCNGC) \tag{B8}$$

$$B2 = f_4\ (WA2C) \tag{B9}$$

$$WBL25 = (B1 + B2) * WA2 \tag{B10}$$

$$WA3 = WA2 - WBL25 \tag{B11}$$

Volume 3. - Two dynamic equations and a state equation are used to calculate the total pressure, temperature, and stored mass (air) in volume 3. The bleed fraction is a function of corrected compressor airflow. A first-order lag equation is used to calculate temperature in this volume. Enthalpy is calculated as a linear function of temperature.

$$WXQ2 = f_5\ (WA2C) \tag{B12}$$

$$WBL3 = (WXQ2 + 0.0025) * WA2 \tag{B13}$$

$$WS3 = \int_0^t (WA3 - WBL3 - WA31)dt + ICWS3 \tag{B14}$$

$$T3L = \int_0^t 1/TAU3 * (T3 - T3L)dt + ICT3 \tag{B15}$$

$$H3 = 928.9 * T3L - 16538.5 \tag{B16}$$

$$P3 = KV3 * WS3 * T3L \tag{B17}$$

Combustor. - The combustor mass flow is a function of inlet pressure, inlet temperature, outlet pressure, and a pressure loss coefficient. The combustor efficiency is a function of fuel-air ratio. The enthalpy increase through the combustor is a function of fuel-air ratio, combustor efficiency, and fuel properties.

$$WA31 = [P3 * (P3 - P41)/(KDPB * T3)]^{1/2} \tag{B18}$$

$$WF = WFPH/3600 \tag{B19}$$

$$FAR = WF/WA31 \tag{B20}$$

$$EFFB = f_6\ (FAR) \tag{B21}$$

$$DHB = FAR * EFFB * HVF \tag{B22}$$

$$H41 = (H3 + DHB)/(1. + FAR) \tag{B23}$$

Volume 41 (combustor outlet). - The temperature in volume 41 is calculated as a linear function of enthalpy. The state equation is combined with a dynamic continuity equation to calculate pressure.

$$T41 = 8.926E-4 * H41 + 180.4 \tag{B24}$$

$$P41 = \int_0^t KV41 * T41 * (WA31 + WF - W41)dt + ICP41 \tag{B25}$$

Gas generator turbine. - In prior simulations (refs. 5 to 7) turbine performance was represented by an enthalpy drop parameter and a flow parameter that were both bivariable functions of pressure ratio and corrected speed. However, for this engine the turbine data obtained from the manufacturer's engine performance program were worked into a simpler functional form. By using a critical velocity parameter (ref. 9), an enthalpy drop parameter was obtained that was a function of only pressure ratio. From these parameters the actual enthalpy drop, exit enthalpy, and temperature can be calculated. Because over the operating range of interest this turbine was found to be choked, a simple choked nozzle equation was used to calculate flow.

$$PRGT = P45/P41 \tag{B26}$$

$$DHQTH4 = f_7\ (PRGT) \tag{B27}$$

$$THTA41 = 2.9322E-3 * T41 + 0.0856 \tag{B28}$$

$$DHGT = DHQTH4 * THTA41 \tag{B29}$$

$$H44 = H41 - DHGT \tag{B30}$$

$$W41 = KWGT * P41/THTA41 \quad (B31)$$

Volume 45 (interturbine). - In volume 45 bleed cooling flow is mixed with gas generator turbine exit flow. The enthalpy of the mixed gases is assumed to be proportional to the enthalpy of the turbine exit gas. The temperature is calculated as a linear function of enthalpy. The state equation is combined with a dynamic continuity equation to calculate pressure.

$$H45 = 0.96 * H44 \quad (B32)$$

$$T45 = 9.456E-4 * H45 + 111.9 \quad (B33)$$

$$P45 = \int_0^t KV45 * T45 * (W41 - W45 + 0.7826 * WXQ2 * WA2) \quad (B34)$$

Power turbine. - For this turbine an enthalpy drop parameter and a flow parameter are obtained that are functions of only the pressure ratio across the turbine. By using these parameters and the critical velocity parameter for this turbine, the enthalpy drop, exit enthalpy, exit temperature, and weight flow can be calculated

$$PRPT = P49/P45 \quad (B35)$$

$$DHQTH5 = f_8 (PRPT) \quad (B36)$$

$$THTA45 = 2.9322E-3 * T45 + 0.0856 \quad (B37)$$

$$DHPT = DHQTH5 * THTA45 \quad (B38)$$

$$H49 = H45 - DHPT \quad (B39)$$

$$T49 = 9.448E-4 * H49 + 107.7 \quad (B40)$$

$$W45C = f_9 (PRPT) \quad (B41)$$

$$W45 = W45C * P45/THTA45 \quad (B42)$$

Compressor and gas generator turbine rotor. - The torques of these components are calculated from the changes in the fluid energy from input to output. For the compressor an empirical relationship is used to account for interstage compressor bleed. The rotor speed is determined from a dynamic angular momentum equation.

$$TORQCM = KTRQ/NG * [0.29 * H3 * WA3 + (0.71 * H3 - H2) * WA2] \quad (B43)$$

$$TORQGT = KTRQ/NG * DHGT * W41 \quad (B44)$$

$$NG = \int_0^t KINR/IGT * (TORQGT - TORQCM)dt + ICNG \quad (B45)$$

$$NGC = NG/\sqrt{TH2} \quad (B46)$$

Power turbine and load rotor. - The power turbine torque and rotor speed are calculated by using the same types of equations as above. The load torque is determined as a function of load-demand spindle angle LDS and is speed dependent.

$$TORQPT = KTRQ/NP * DHPT * W45 \tag{B47}$$

$$TORQLD = [50.843 - LDS * (0.0835 - 0.1018 * LDS)] * (NP/20000.) ** 2 \tag{B48}$$

$$NP = \int_0^t KINR/IPT * (TORQPT - TORQLD)dt + ICNP \tag{B49}$$

Control Components

Electrical Control Unit

T45 thermocouple harness. - The dynamics of the T45 thermocouple harness are represented by two first-order lags. One of the time constants is fixed and the second is a bivariable function of the temperature and flow parameter at station 45.

$$T45E = T45 + T45COR \tag{B50}$$

$$W45R = W45 * T45/P45 \tag{B51}$$

$$TC45H = f_{10}\ (W45R, T45) \tag{B52}$$

$$T45L = \int_0^t 1/TC45 * (T45E - T45L)dt + ICT45E \tag{B53}$$

$$T45EL = \int_0^t 1/TC45H * (T45L - T45EL)dt + ICT45E \tag{B54}$$

T45 limit control. - In this control the sensed temperature T45 is compared with a limit value to give an error signal. This signal then goes through a first-order lag and a lead-lag circuit to give a compensated T45 error signal.

$$TERR = T45EL - T45LIM \tag{B55}$$

$$TSGE = \int_0^t KT45LM/TC45L * (TERR - TSGE)dt + ICTSGE \tag{B56}$$

$$TSGL = \int_0^t KTSG1/TC45LG * (TSGE - TSGL)dt + ICTSG1 \tag{B57}$$

$$TSIG = TC45LD * (TSGE - TSGL)/TC45LG \tag{B58}$$

NP speed control. -In this control the sensed speed NP is compared with a reference value to given an error signal. This signal then goes through a

lead-lag and first-order lag to give a compensated NP error signal. Additional gain and error rate compensation is added if the error signal is larger than a small threshold value.

$$SPDER = PCNPS - PCNPRF \tag{B59}$$

$$SPDR = \begin{cases} SPDER - SPDB & \text{for } SPDER > SPDB \\ 0.0 & \text{for } -SPDB < SPDER < SPDB \\ SPDER + SPDB & \text{for } SPDER < -SPDB \end{cases} \tag{B60}$$

$$SPDL = \int_0^t 1/TCGRLG * (SPDR - SPDL)dt + 0.0 \tag{B61}$$

$$SPDRC = \int_0^t 1/TCGRLD * (SPDL - SPDRC)\, dt + 0.0 \tag{B62}$$

$$SPDR2 = KGVNR * (SPDL - SPDRC)/TCGRLD \tag{B63}$$

$$SPDS1 = KNTRM * SPDER + KNGVN * SPDR + SPDR2 \tag{B64}$$

$$SPDS2 = 2.0 * SPDS1 \tag{B65}$$

$$SPDS = \int_0^t KSPDS/TCGVLG * (SPDS2 - SPDS)dt + 0.0 \tag{B66}$$

$$SPDSL = TCGVLD * (SPDS2 - SPDS)/TCGVLG \tag{B67}$$

$$SPDSF = \int_0^t 1/TCGVLG * (SPDSL - SPDSF)dt + 0.0 \tag{B68}$$

Speed-temperature limit selector. - This selector logic normally selects the speed error signal. If the temperature error indicates T45 over-temperature, the logic selects the error signal that will give lowest fuel flow.

$$TSIGS = \begin{cases} TSIG & \text{for } TSIG > 0.0 \\ 0.0 & \text{for } TSIG < 0.0 \end{cases} \tag{B69}$$

$$SPDSS = \begin{cases} TSIGS & \text{for } TSIGS > SPDSF \\ SPDSF & \text{for } TSIGS < SPDSF \end{cases} \tag{B70}$$

Principal ECU compensation. - The ECU compensation circuit contains parallel proportional and integral paths followed by a first-order lag. The integrated error signal is limited if it exceeds maximum or minimum values.

$$SPDSP = KPROP * SPDSS \tag{B71}$$

$$SPDSI = \int_0^t (KINTG * SPDSS)dt + ICSPDI \tag{B72}$$

$$SPDSIL = \begin{cases} SPDSHL & \text{for } SPDSI > SPDSHL \\ SPDSI & \text{for } SPDSLL < SPDSI < SPDSHL \\ SPDSLL & \text{for } SPDSI < SPDSLL \end{cases} \quad (B73)$$

$$SPDG = \int_0^t 1/TCSPDG * (SPDSIL + SPDSP - SPDG)dt + ICSPDG \quad (B74)$$

Hydromechanical Control Unit

The primary function of the hydromechanical control unit is to control the fuel flow to the engine by positioning the fuel-metering valve. The valve position is affected by a combination of pilot-initiated inputs, sensed engine variables, and an electrical trim signal from the ECU. The valve position is also constrained by an idle schedule, an acceleration schedule, a deceleration schedule, and maximum and minimum absolute fuel flow limits. In the following description the fuel flow demand parameter WFPDM is the primary control variable. Fuel valve position and fuel flow are proportional to this parameter multiplied by the sensed compressor discharge pressure PS3L.

Topping line. - A maximum value of the fuel flow demand parameter is calculated as a function of compressor inlet temperature T2.

$$WFPTP = f_{11}(T2) \quad (B75)$$

Gas generator turbine speed and droop line. - An incremental fuel flow demand parameter is calculated from the difference between sensed speed NG and 101 percent of design speed. This provides NG droop compensation through proportional feedback control.

$$PCNG = NG/NGDSN * 100 \quad (B76)$$

$$PCNGS = \int_0^t 1/TCNGS * (PCNG - PCNGS)dt + ICPCNG \quad (B77)$$

$$WFPDRP = KNDRP * (101. - PCNGS) \quad (B78)$$

Power-available spindle input. - This pilot-initiated input determines another incremental fuel flow demand parameter. This in effect sets the maximum available gas generator turbine speed and the maximum available power.

$$WFPRF = f_{12}(PAS) \quad (B79)$$

Load-demand spindle input. - This pilot-initiated input changes the collective pitch of the aircraft rotor system and thus changes the load on the power turbine. It also provides a feedforward signal (effectively another incremental fuel flow demand parameter) to rapidly change NG in anticipation of the load change.

$$PCNGD = f_{13}(LDS) \quad (B80)$$

$$WFQD = f_{14}(LDS) \quad (B81)$$

$$DWFPL = KWLDSR - WFQI + KNDRP * (101. - PCNGD) \quad (B82)$$

Torque motor. - The torque motor receives a trim demand signal from the ECU. This signal is compared with a position feedback signal to produce an error signal. The error signal goes through a first-order lead-lag circuit and is amplified to provide a voltage that is applied to the torque motor coil. The resulting torque motor current moves the flapper valve to a position that will provide a null current (within a deadband) through the position feedback signal. The flapper valve movement is constrained by position limits and is amplified mechanically to provide a fuel flow demand trim signal.

$$TMSE = SPDG - KTMFB * TMLO - TMBS1 \quad (B83)$$

$$TMSR = \int_0^t KTMSR/TCTMSR * (TMSE - TMSR)dt + ICTMSR \quad (B84)$$

$$TMSL = TMSE + TMSR \quad (B85)$$

$$TMSLL + KTMC * TMSL \quad (B86)$$

$$TMI = \begin{cases} TMILIM & \text{for } TMSLL > TMILIM \\ TMSLL - TMBS2 & \text{for } -TMILIM < TMSLL < TMILIM \\ -TMILIM & \text{for } TMSLL < -TMILIM \end{cases} \quad (B87)$$

$$TMSIG = \begin{cases} TMI - TMDB & \text{for } TMI > TMDB \\ 0.0 & \text{for } -TMDB < TM1 < TMDB \\ TMI + TMDB & \text{for } TMI < -TMDB \end{cases} \quad (B88)$$

$$TMLO = \int_0^t (KTMLO * TMSIG)dt + ICTMLO \quad (B89)$$

$$TMLOL = \begin{cases} TMLMAX & \text{for } TMLO > TMLMAX \\ TMLO & \text{for } TMLMIN < TMLO < TMLMAX \\ TMLMIN & \text{for } TMLO < TMLMIN \end{cases} \quad (B90)$$

$$TMRU = KTMRU * TMLOL \quad (B91)$$

Fuel flow demand parameter. - A combined fuel flow demand parameter is obtained by summing the topping line value and the incremental values from the other inputs. The feedforward signal from the LDS input and the trim signal from the torque motor are summed, and the sum is limited to positive values. Because this signal is subtracted from the other inputs, it can only trim down.

$$RULDS = \begin{cases} DWFPL + TMRU & \text{for } (DWFPL + TMRU) > 0.0 \\ 0.0 & \text{for } (DWFPL + TMRU) < 0.0 \end{cases} \quad (B92)$$

$$WFPDM = WFPTP + WFPDRP - WFPRF - RULDS \quad (B93)$$

Idle schedule. - This schedule determines a limiting value of fuel flow demand parameter for PAS in the ground-idle region ($23.5 < PAS < 28.5$). This parameter is a function of NG and T2.

$$WFIRF = f_{15}(T2) \tag{B94}$$

$$PCNGI = f_{16}(T2) \tag{B95}$$

$$WFIDM = KNDRP * (PCNGI - PCNGS) + WFIRF \tag{B96}$$

Acceleration schedule. - This schedule determines a limiting value of fuel flow demand parameter during engine acceleration. This parameter is a bivariable function of NG and T2.

$$WFPAC = f_{17}(PCNGS, T2) \tag{B97}$$

Deceleration schedule. - This schedule determines a limiting value of fuel flow demand parameter during engine deceleration. This parameter is a function of NG.

$$WFPDC = \begin{cases} WFPDCH & \text{for } PCNGS > PCNGDH \\ KWFD * (PCNGS - PCNGDL) & \text{for } PCNGDL < PCNGS < PCNGDH \\ WFPDCL & \text{for } PCNGS < PCNGDL \end{cases} \tag{B98}$$

Select logic - fuel flow demand parameter. - This logic selects the final fuel flow demand parameter by considering the limiting values determined by the schedules.

$$WFPD0 = \begin{cases} WFPDM & \text{for } WFPDM > WFIDM \\ WFIDM & \text{for } WFPDM < WFIDM \end{cases} \tag{B99}$$

$$WFPD1 = \begin{cases} WFPD0 & \text{for } WFPD0 < WFPAC \\ WFPAC & \text{for } WFPD0 > WFPAC \end{cases} \tag{B100}$$

$$WFPD2 = \begin{cases} WFPD1 & \text{for } WFPD1 > WFPDC \\ WFPDC & \text{for } WFPD1 < WFPDC \end{cases} \tag{B101}$$

Compressor static discharge pressure sensor. - The response of this sensor is considered to be a first-order lag.

$$PS3L = \int_0^t 1/TCPS3 * (PS3 - PS3L)dt + ICPS3 \tag{B102}$$

Fuel-flow-metering valve. - Mechanical stops on this valve limit the fuel flow to maximum and minimum values.

$$WFMV = WFPD2 * PS3L \tag{B103}$$

$$WFPH = \begin{cases} WFMAX & \text{for } WFMV > WFMAX \\ WFMV & \text{for } WFMIN < WFMV < WFMAX \\ WFMIN & \text{for } WFMV < WFMIN \end{cases} \tag{B104}$$

APPENDIX C

ANALOG DIAGRAMS AND DIGITAL FLOW CHART

Flow Chart of Function Generation Program

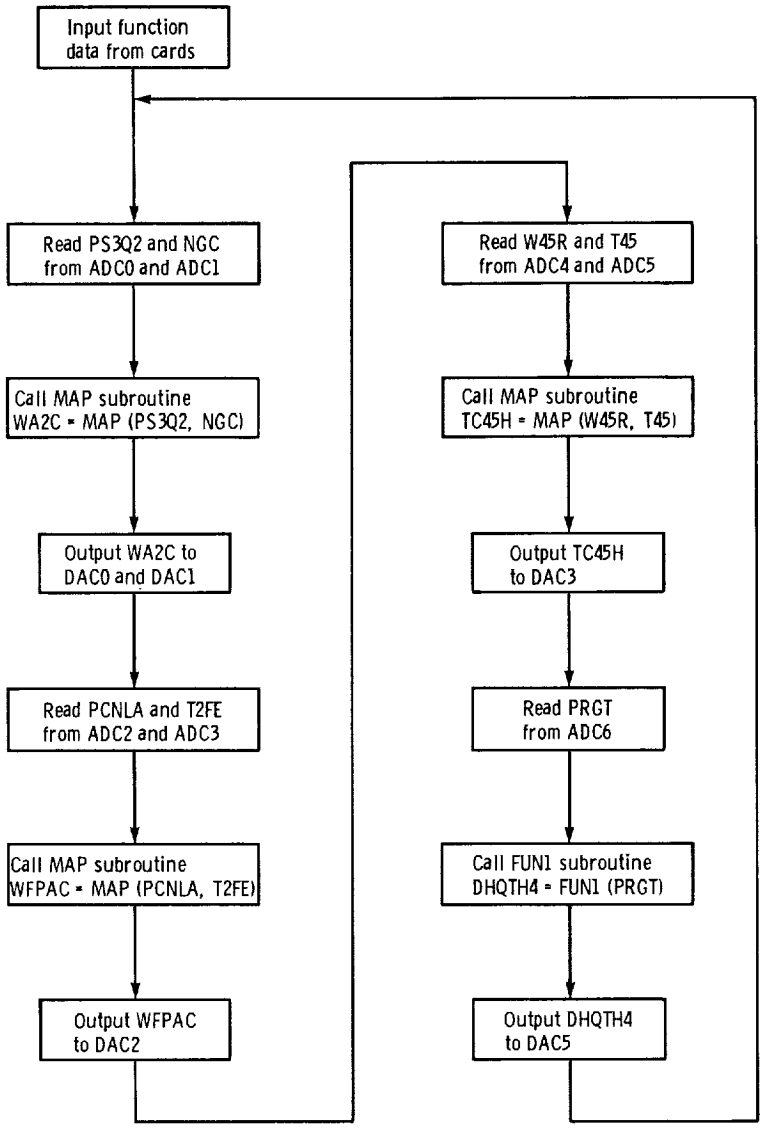

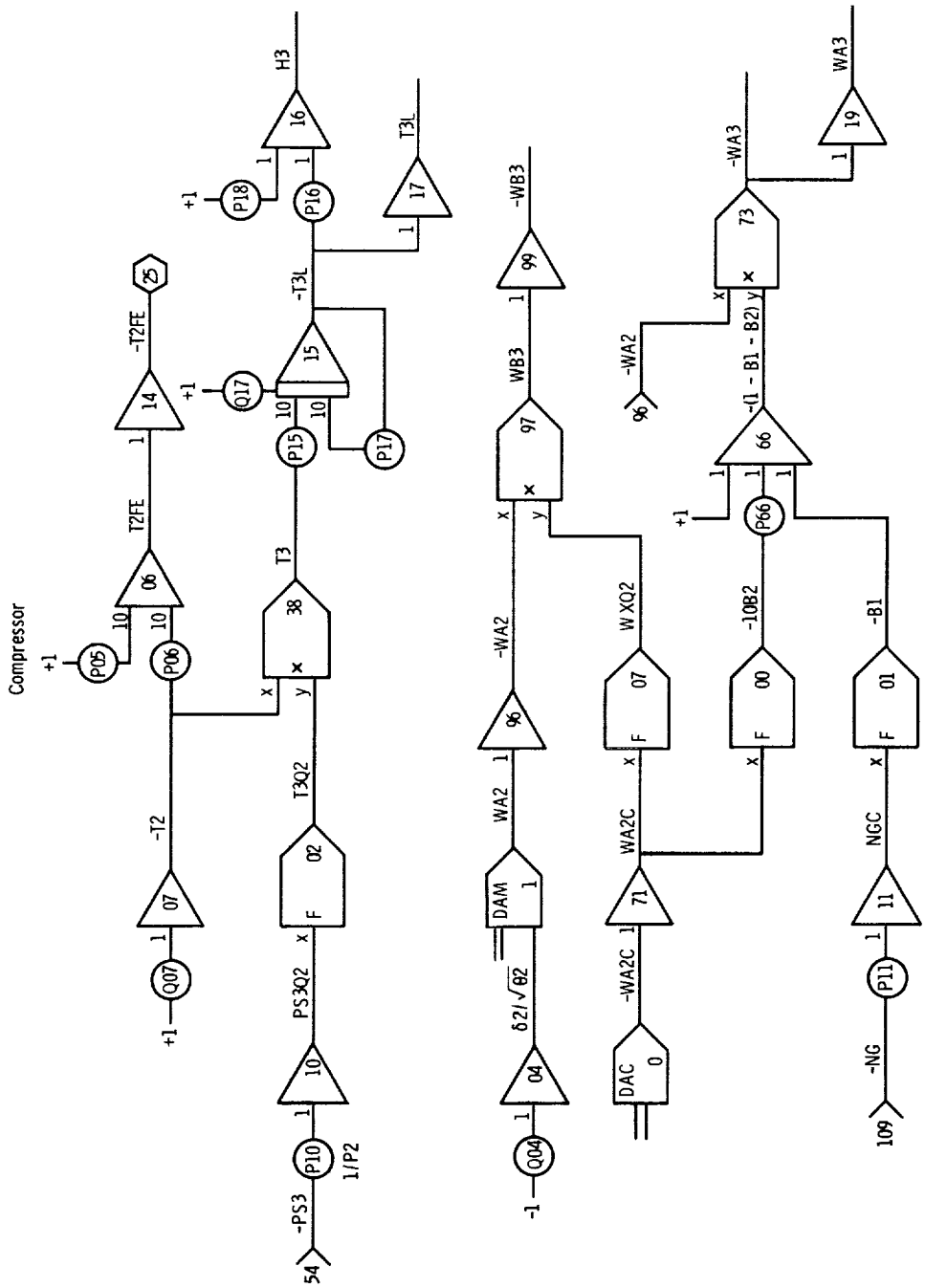
Compressor
+1
P05
10
P06
10
06
T2FE
1
14
-T2FE
25
-T2
1
07
Q07
+1
x
y
T3
38
T3Q2
F
02
PS3Q2
x
10
1
P10
1/P2
-PS3
54
+1
P18
1
16
H3
-T3L
+1
Q17
15
10
10
P15
P17
1
17
T3L
-WB3
99
1
WB3
97
x
y
-WA2
96
1
WA2
DAM
1
δ2/√θ2
1
Q04
-1
W XQ2
07
F
x
WA2C
71
1
-WA2C
DAC
0
-WA3
73
x
y
-(1 - B1 - B2)
66
1
1
P66
1
+1
-10B2
00
F
x
-WA2
96
WA3
19
1
-B1
01
F
x
NGC
11
1
P11
1
-NG
109

Compressor and Combustor

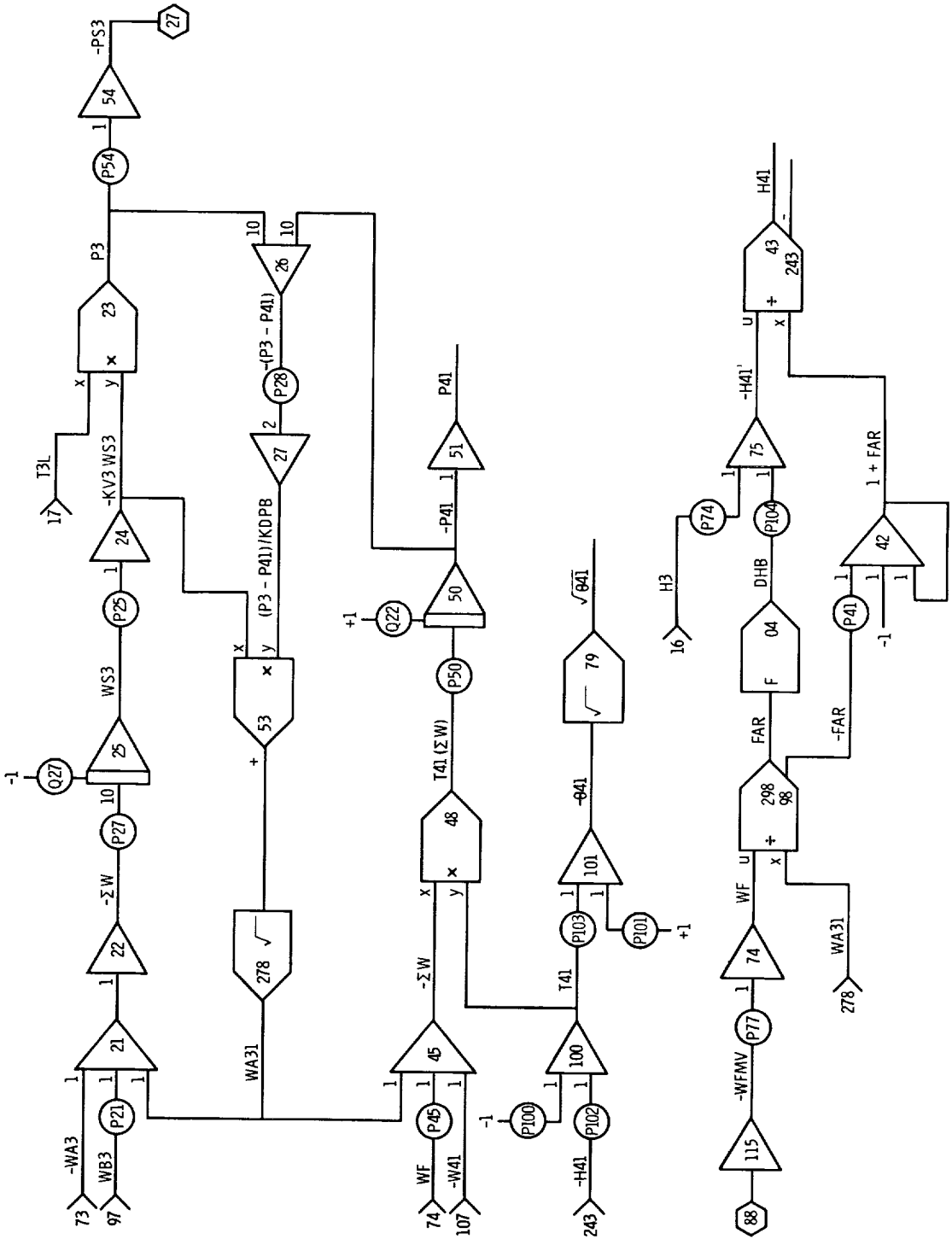

Gas Generator and Power Turbines

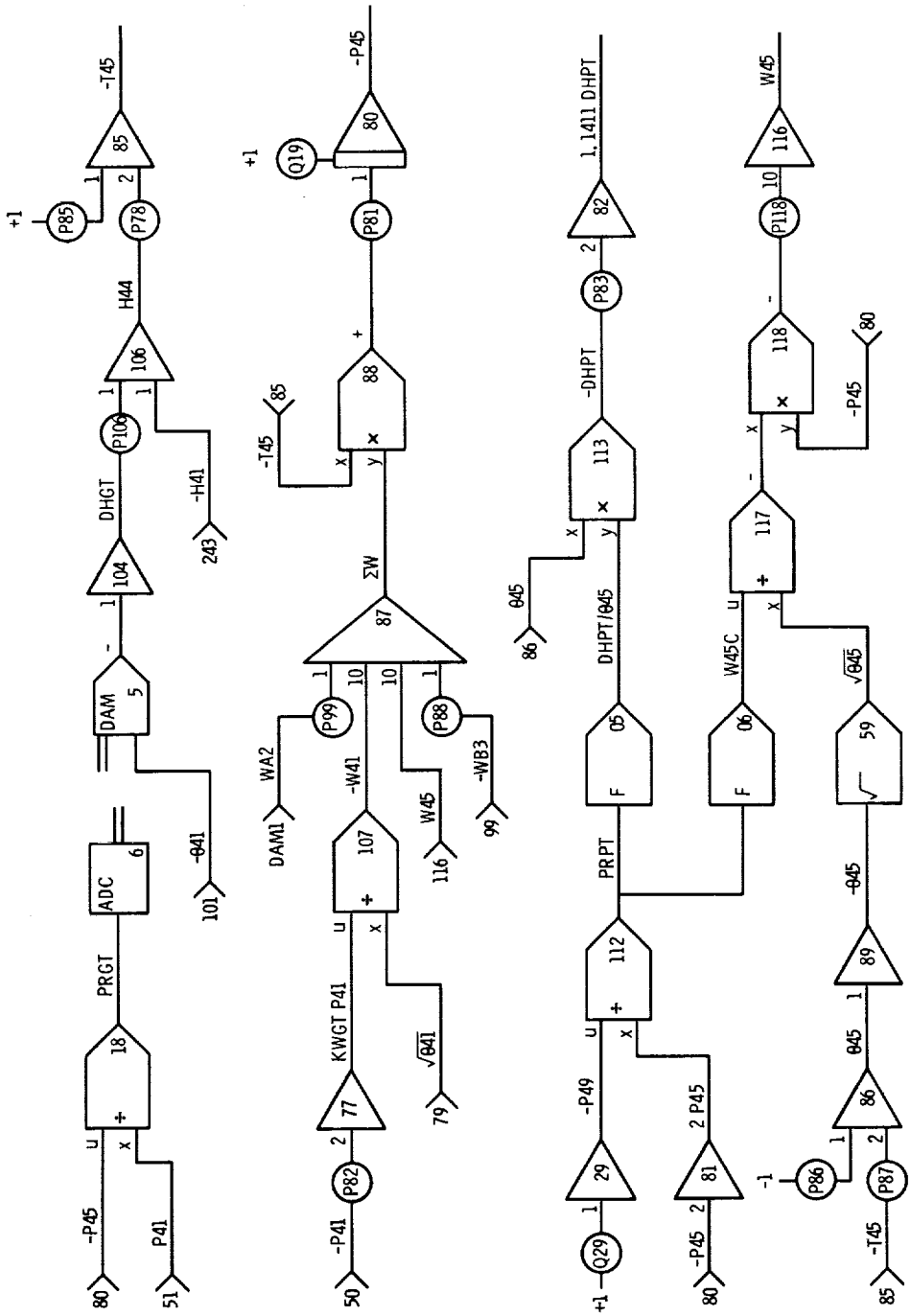

Torques and Speeds

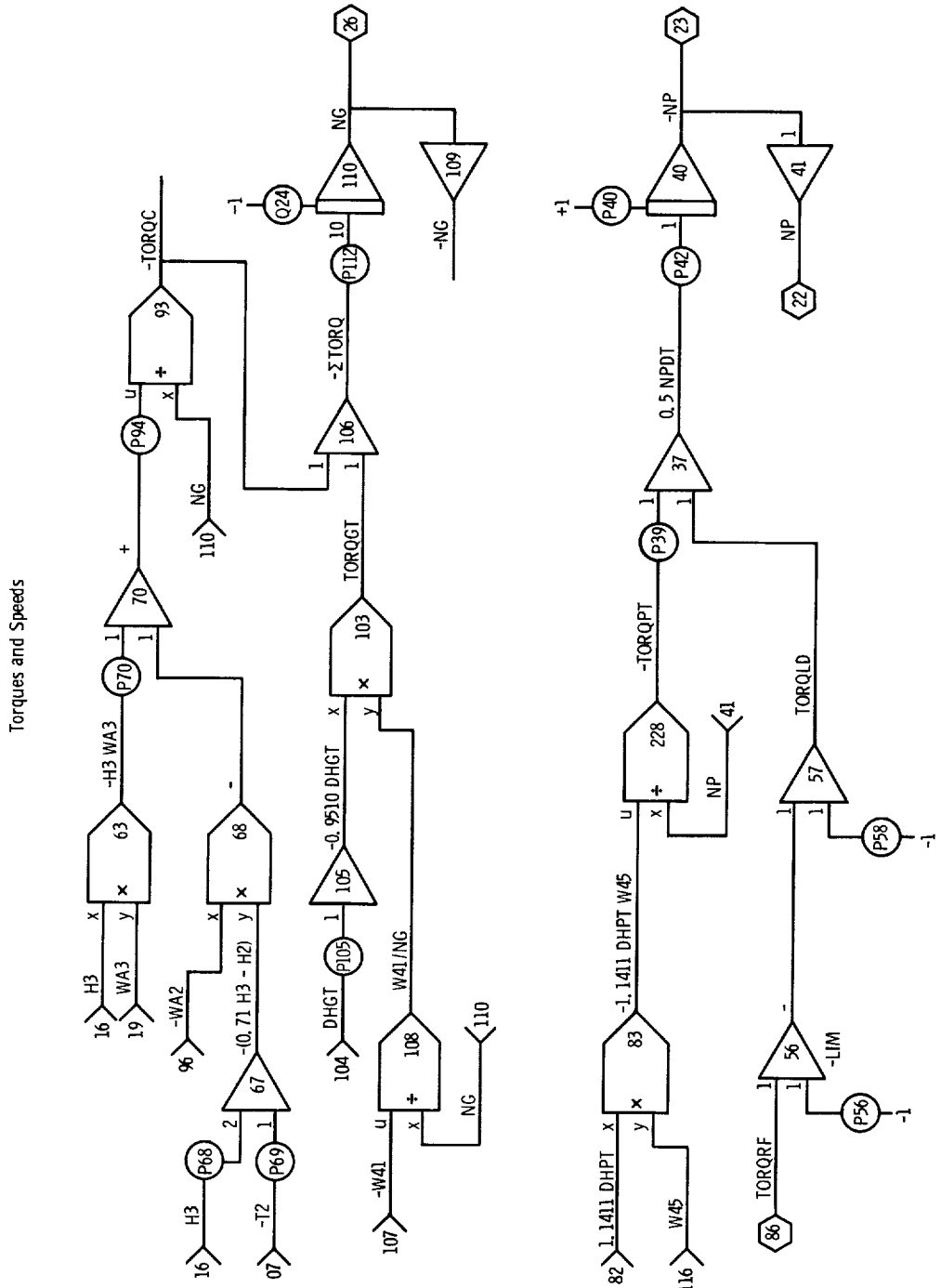

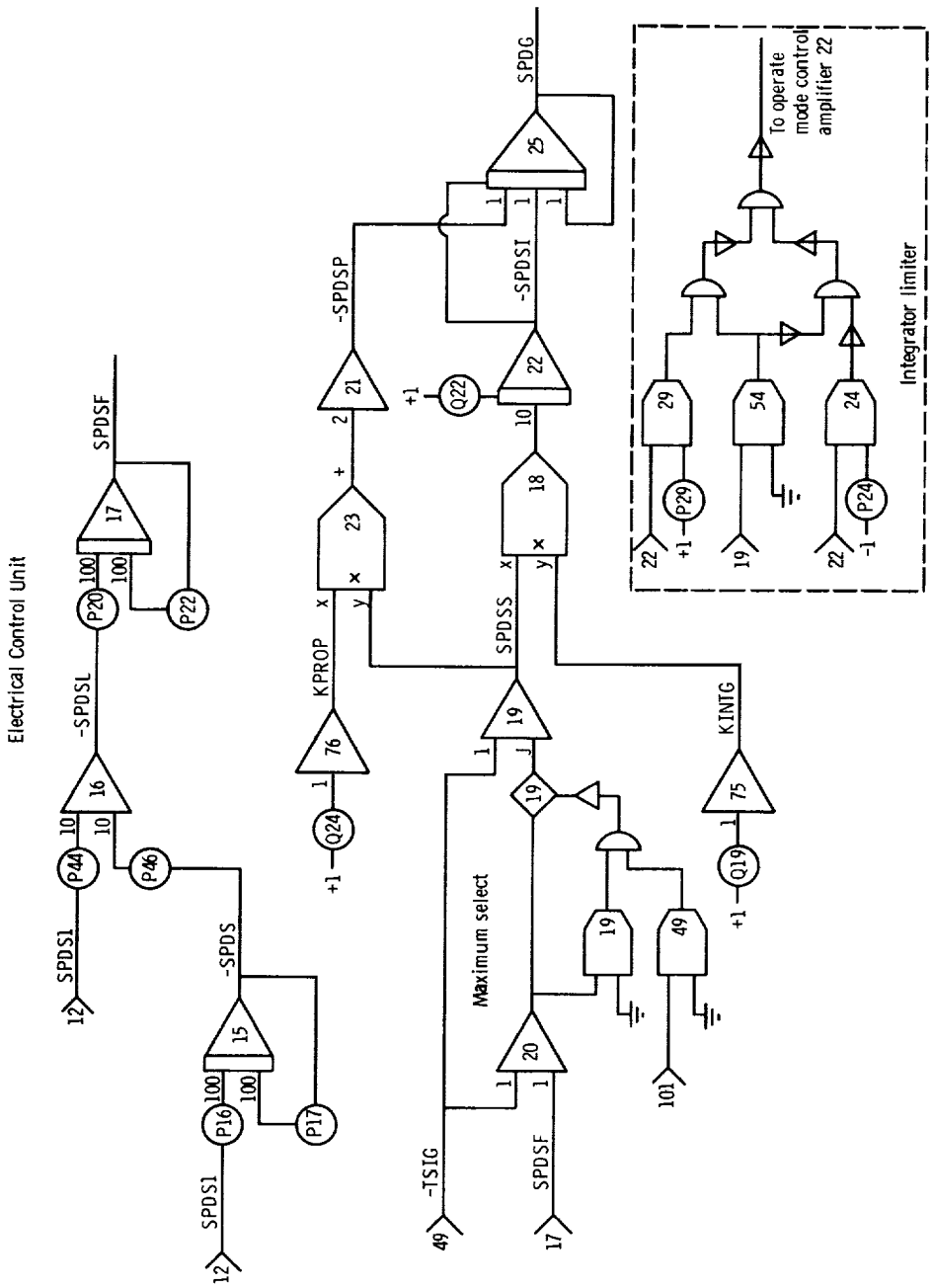
Electrical Control Unit
SPDSI
12
P44
P46
-SPDSL
16
SPDSF
17
P20
P22
-SPDS
15
P16
P17
SPDSI
12
KPROP
76
Q24
+1
-SPDSP
21
23
+1
Q22
22
-SPDSI
SPDG
25
SPDSS
18
19
Maximum select
-TSIG
49
SPDSF
17
20
19
19
49
101
KINTG
75
Q19
+1
To operate mode control amplifier 22
Integrator limiter
29
P29
+1
22
54
19
24
P24
-1
22

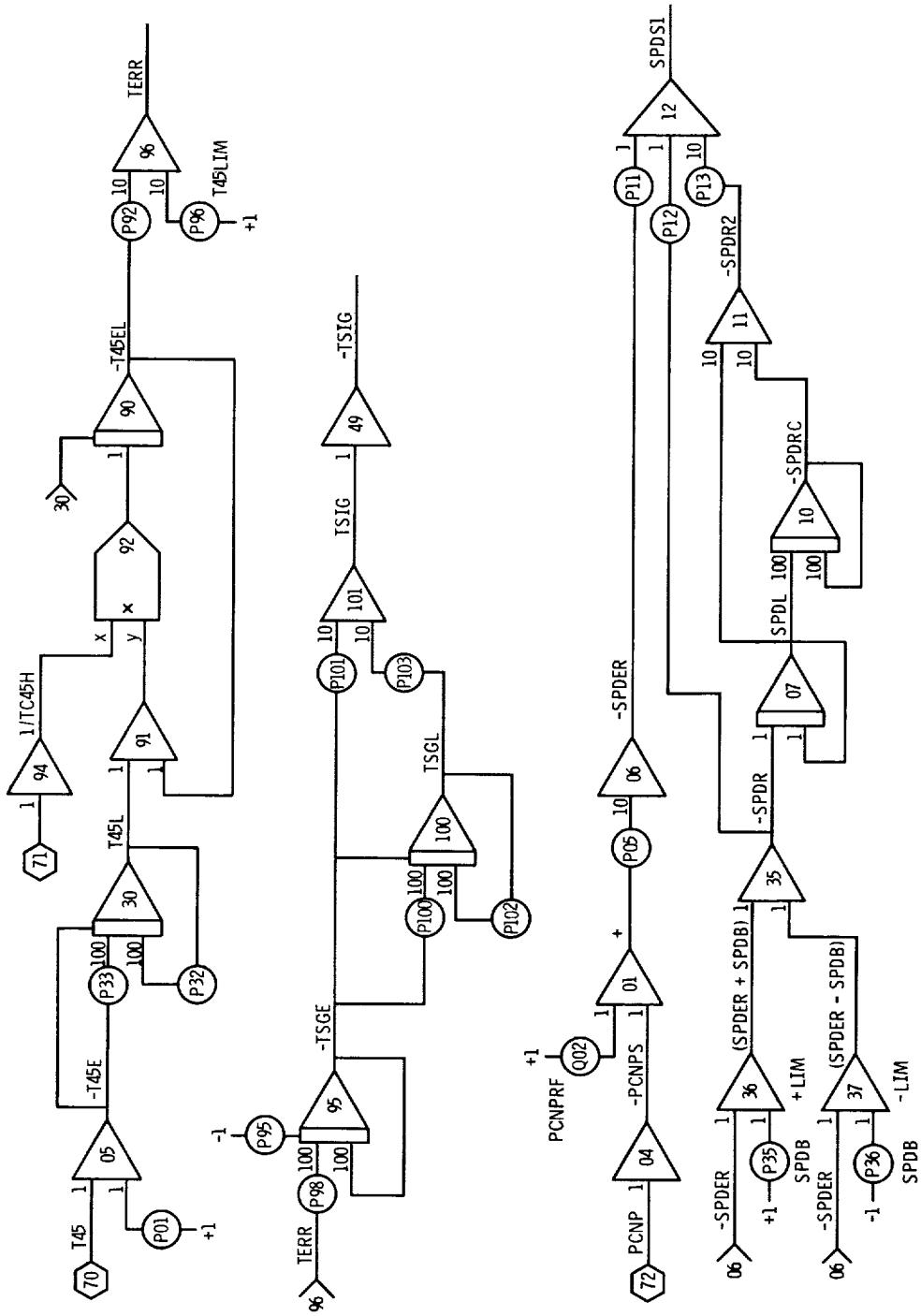
T45
70
05
-T45E
P01
+1
P33
P32
100
100
30
T45L
71
94
1/TC45H
91
92
x
y
90
-T45EL
30
96
IERR
P92
P96
T45LIM
+1
-1
P95
95
-TSGE
P98
TERR
96
P101
101
TSIG
49
-TSIG
P103
TSGL
100
P100
P102
PCNPRF
Q02
01
-PCNPS
04
PCNP
72
06
-SPDER
P05
P11
P12
12
SPDS1
P13
-SPDR2
11
-SPDRC
10
SPDL
07
-SPDR
35
(SPDER + SPDB)
36
+LIM
SPDB
(SPDER - SPDB)
37
-LIM

Hydromechanical Control Unit

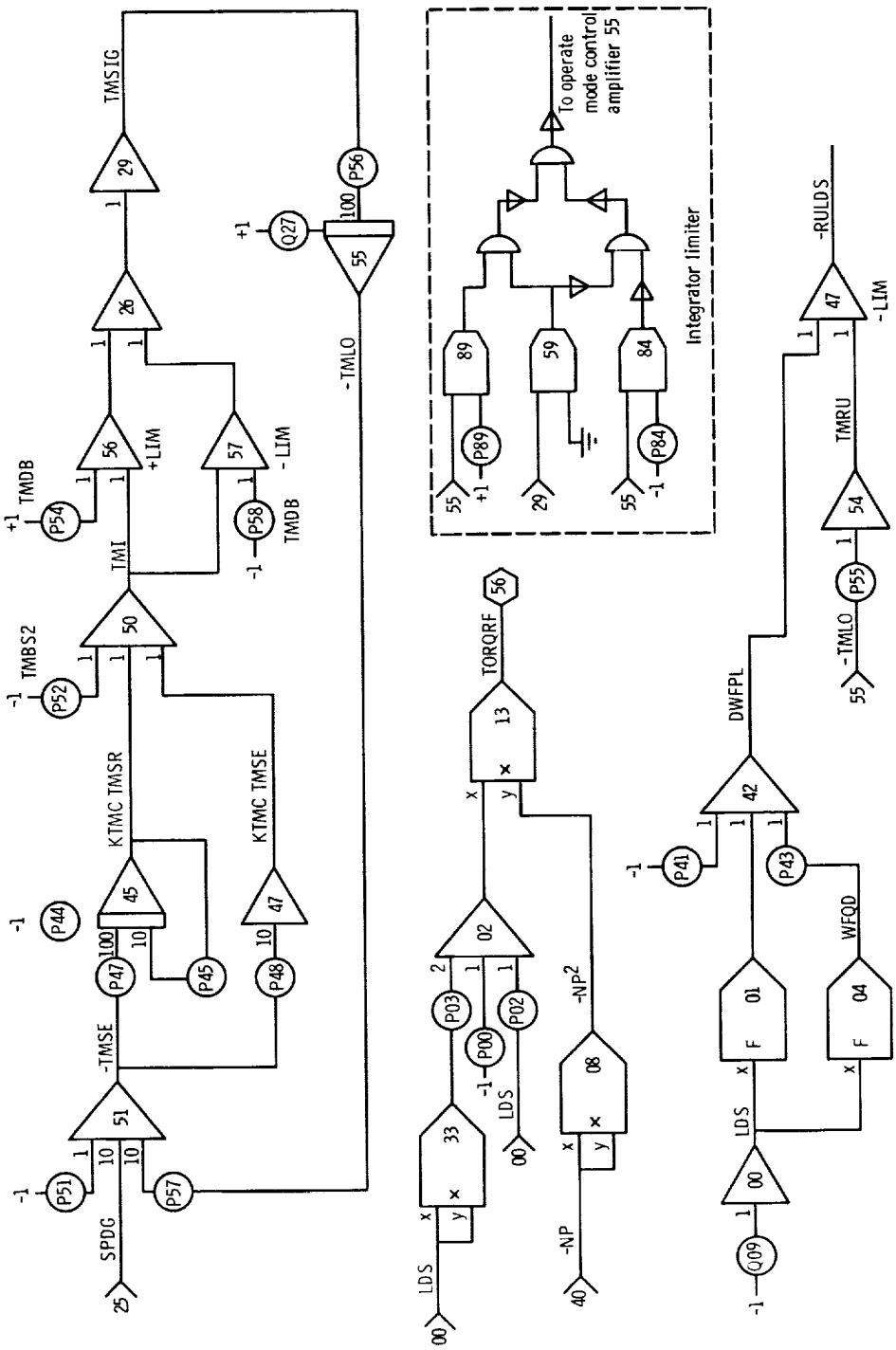

Hydromechanical Control Unit

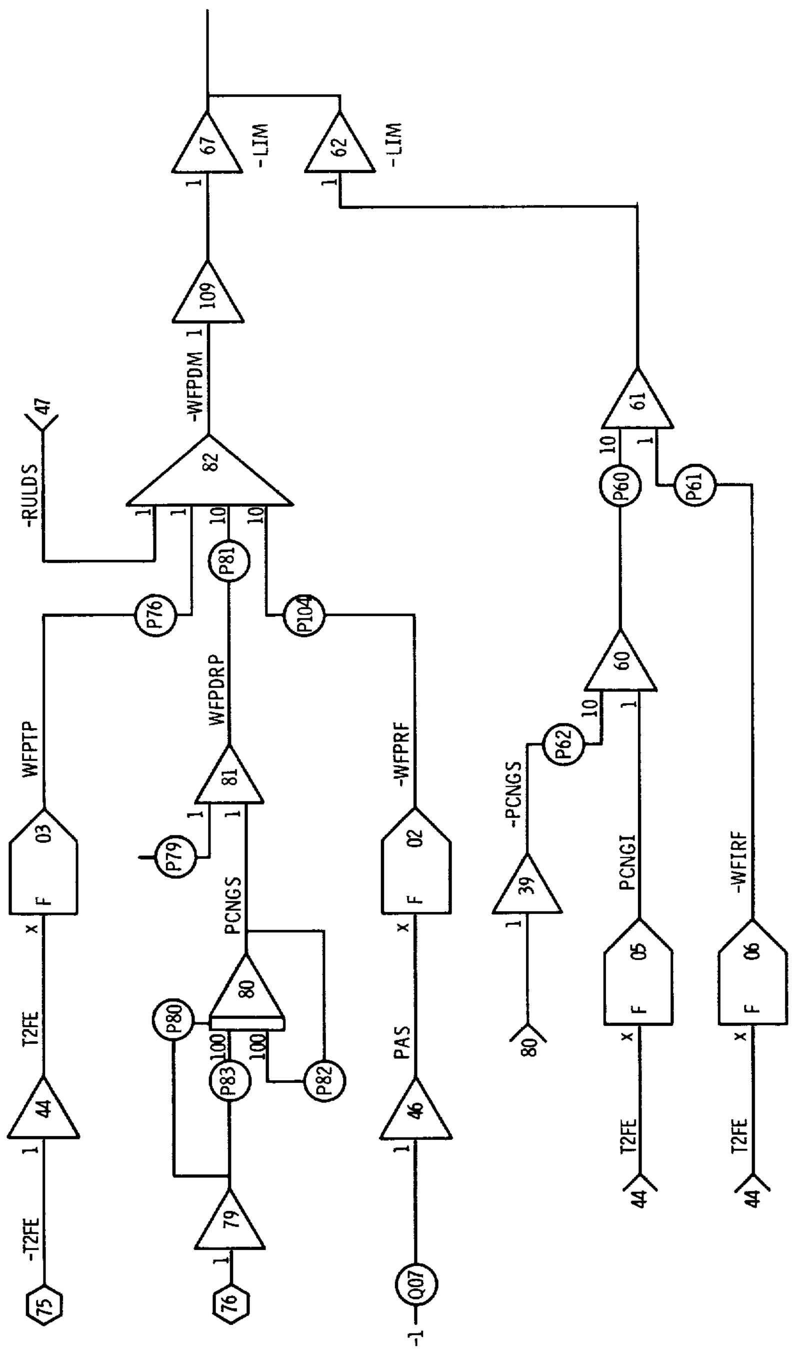

Hydromechanical Control Unit

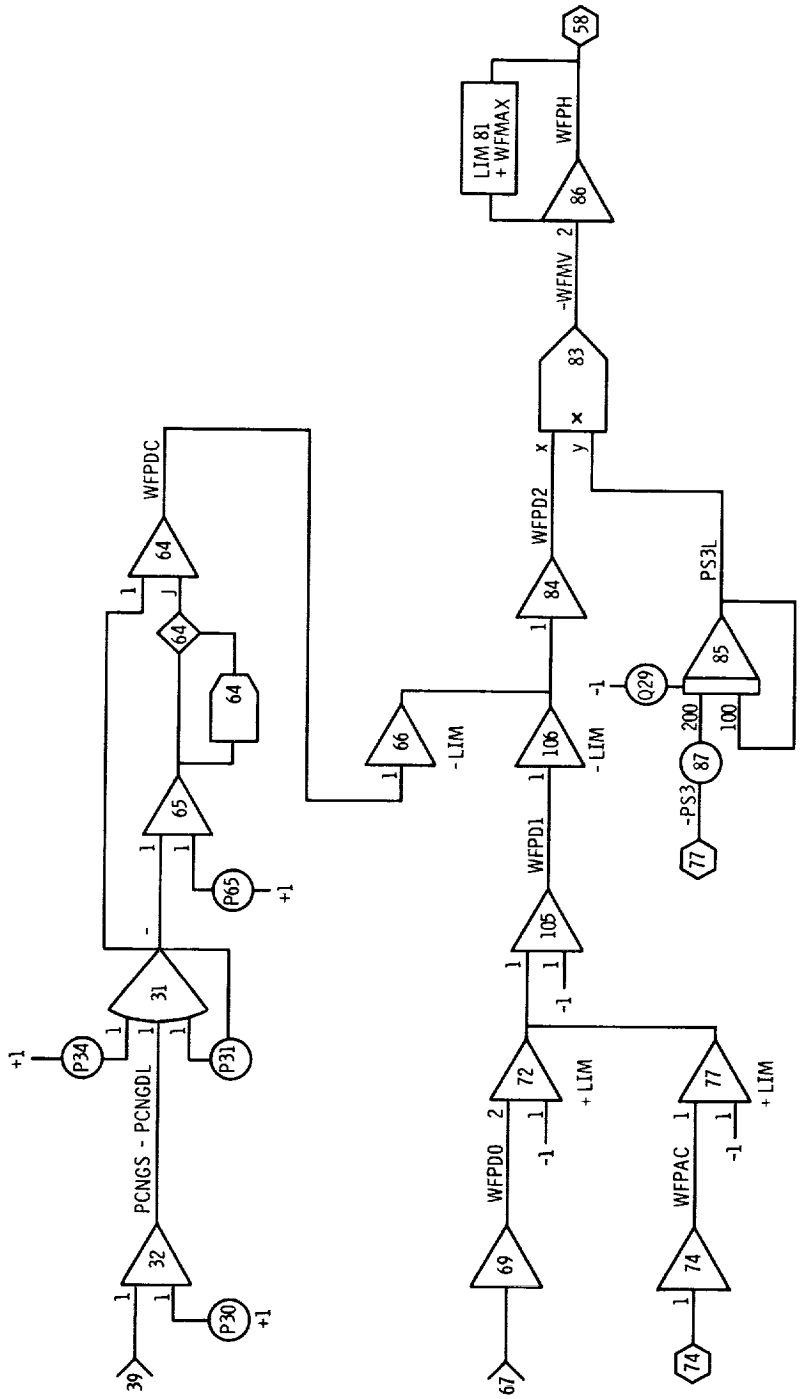

Miscellaneous and A/D and D/A Interface

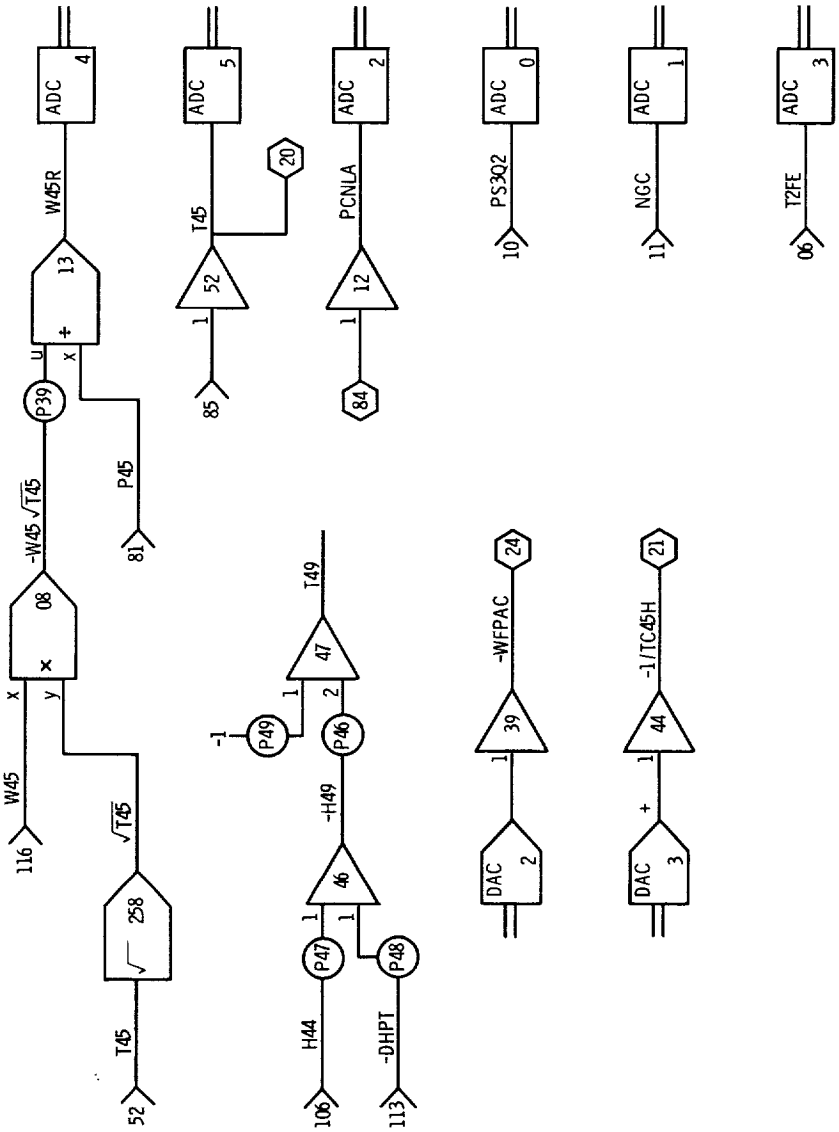

REFERENCES

1. Quiet Clean Short-Haul Experimental Engine (QCSEE) Under-the-Wing Engine Digital Control System Design Report. (R75AEG483, General Electric Co.; NASA Contract NAS3-18021). NASA CR-134920, 1978.

2. Vizzini, R. W.; Lenox, T. G.; and Miller, R. J.: Full Authority Digital Electronic Control Turbofan Engine Demonstration. SAE Paper 801199, Oct. 1980.

3. Szuch, J. R.: Application of Real-Time Engine Simulations to the Development of Propulsion System Controls. AIAA Paper 75-1176, Sept. 1975.

4. Szuch, J. R.; Skira, C.; and Soeder, J. F.: Evaluation of an F100 Multivariable Control Using a Real-Time Engine Simulation. AIAA paper 77-835, July 1977.

5. Seldner, K.; Mihaloew, J. R.; and Blaha, R. J.: Generalized Simulation Technique for Turbojet Engine System Analysis. NASA TN D-6610, 1972.

6. Szuch, J. R.; and Bruton, W. M.: Real-Time Simulation of the TF30-P-3 Turbofan Engine Using a Hybrid Computer. NASA TM X-3106, 1974.

7. Szuch, J. R.; and Seldner, K.: Real Time Simulation of F100-PW-100 Turbofan Engine Using the Hybrid Computer. NASA TM X-3261, 1975.

8. Szuch, J. R.: BASIC Data Manipulation and Display System (BDMADS). NASA TM-83328, 1983.

9. Glassman, A. J., ed.: Turbine Design and Application. Vol. 1. NASA SP-290, 1972.

TABLE I. - SELECTED TEST CONDITIONS

Test condition	Compressor inlet total pressure, P2		Compressor inlet total temperature, T2		Power turbine inlet pressure, P49		Load torque, TORQLD		Fuel flow, WF	
							N-m	ft-lbf	kg/hr	lb/hr
	N/cm^2	psia	K	°R	N/cm^2	psia				
1	9.91	14.37	287.1	516.7	9.91	14.37	40.8	30.1	63.5	140.1
2	9.77	14.17	286.4	515.6	9.95	14.43	122.2	90.1	134.8	297.2
3	9.76	14.16	282.4	508.3	9.97	14.46	201.1	148.3	168.7	372.0
4	9.71	14.09	282.2	508.0	10.07	14.60	280.0	206.5	207.9	458.4
5	9.67	14.02	281.8	507.2	10.09	14.63	371.9	274.3	254.3	560.6
6	9.60	13.92	281.8	507.2	10.15	14.72	489.2	360.8	315.0	694.4

TABLE II. - COMPARISON OF STEADY-STATE RESULTS

Test condition	Type of data	Compressor outlet total pressure, P3		Compressor outlet total temperature, T3		Compressor inlet air mass flow, WA2		Rotational speed of compressor, NG, rpm	Rotational speed of power turbine, NP, rpm	Power turbine inlet total temperature, T45		Power turbine outlet total temperature, T49	
		N/cm^2	psia	K	°R	kg/sec	lbm/sec			K	°R	K	°R
1	Experimental	40.0	58.0	462	832	1.45	3.20	29 480	10 995	785	1413	747	1345
	Digital	39.4	57.2	461	830	1.47	3.24	29 481	10 995	773	1392	738	1328
	Hybrid	39.6	57.4	461	830	1.47	3.25	29 580	11 115	767	1380	731	1316
2	Experimental	78.0	113.1	570	1026	2.34	5.16	37 875	19 995	876	1577	779	1402
	Digital	75.5	109.5	563	1013	2.36	5.21	37 862	19 997	880	1584	778	1400
	Hybrid	75.8	110.0	565	1017	2.39	5.27	37 955	20 235	868	1563	764	1376
3	Experimental	95.8	139.0	601	1081	2.79	6.16	39 236	19 995	903	1626	783	1410
	Digital	95.8	139.0	599	1079	2.80	6.17	39 239	19 921	900	1620	768	1383
	Hybrid	96.7	140.3	601	1082	2.83	6.24	39 335	20 212	894	1609	761	1370
4	Experimental	111.1	161.1	626	1127	3.14	6.92	40 409	19 995	962	1731	809	1457
	Digital	110.7	160.6	624	1124	3.13	6.90	40 398	19 788	957	1723	796	1432
	Hybrid	111.4	161.5	626	1126	3.15	6.95	40 465	20 040	956	1721	793	1427
5	Experimental	127.4	184.8	652	1173	3.47	7.66	41 393	19 995	1021	1838	849	1529
	Digital	126.7	183.8	652	1173	3.47	7.65	41 382	19 952	1021	1838	827	1488
	Hybrid	127.0	184.2	652	1173	3.48	7.68	41 405	19 977	1018	1832	823	1482
6	Experimental	146.1	211.9	682	1228	3.86	8.50	42 880	19 995	1097	1974	889	1600
	Digital	146.1	211.9	683	1229	3.86	8.50	42 861	19 998	1099	1979	870	1566
	Hybrid	146.5	212.5	683	1230	3.87	8.54	42 970	20 107	1093	1968	864	1556

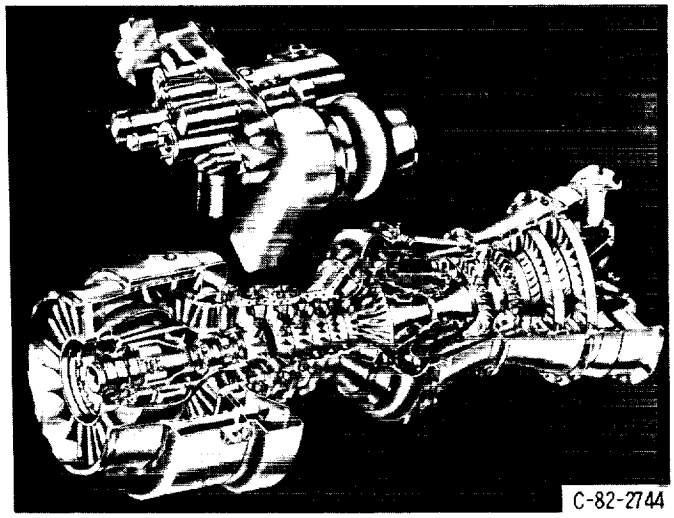

Figure 1. - Small turboshaft engine.

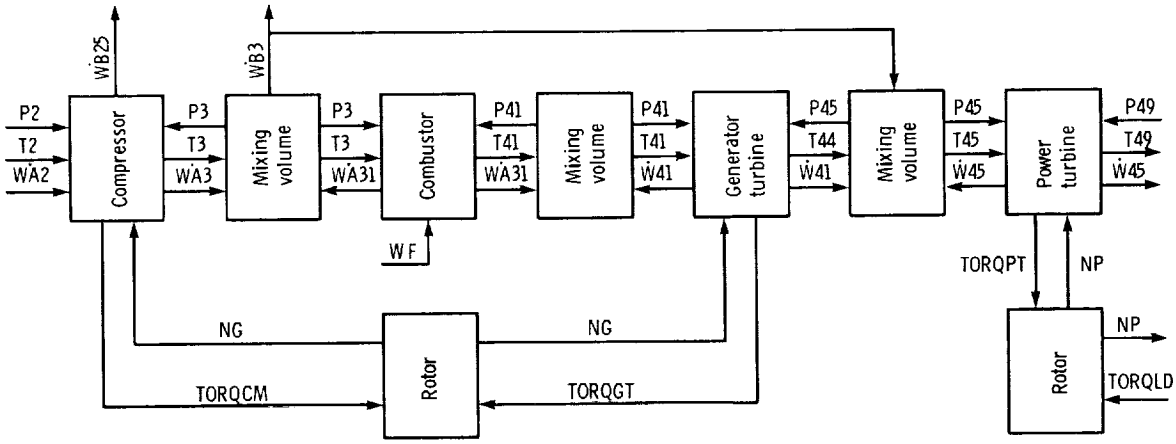

Figure 2. - Block diagram of small turboshaft engine.

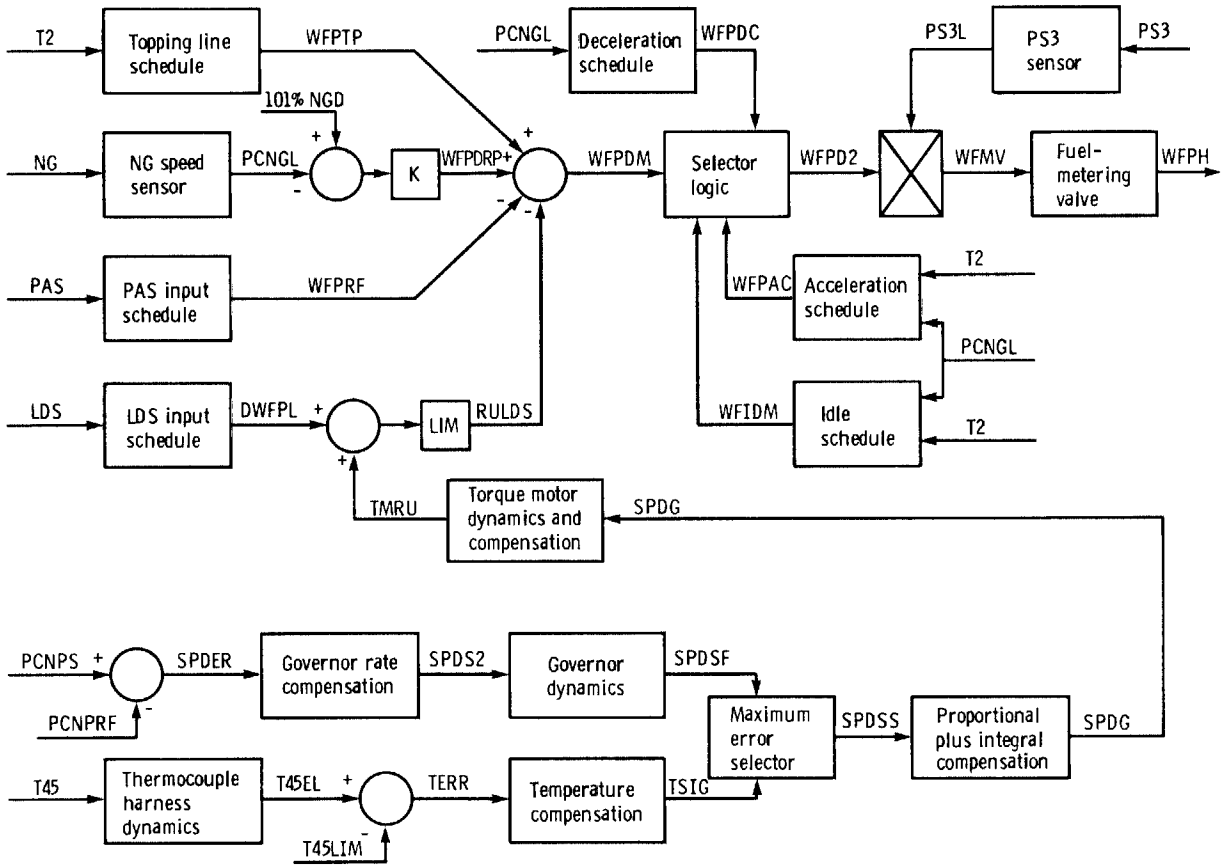

Figure 3. - Block diagram of engine control system.

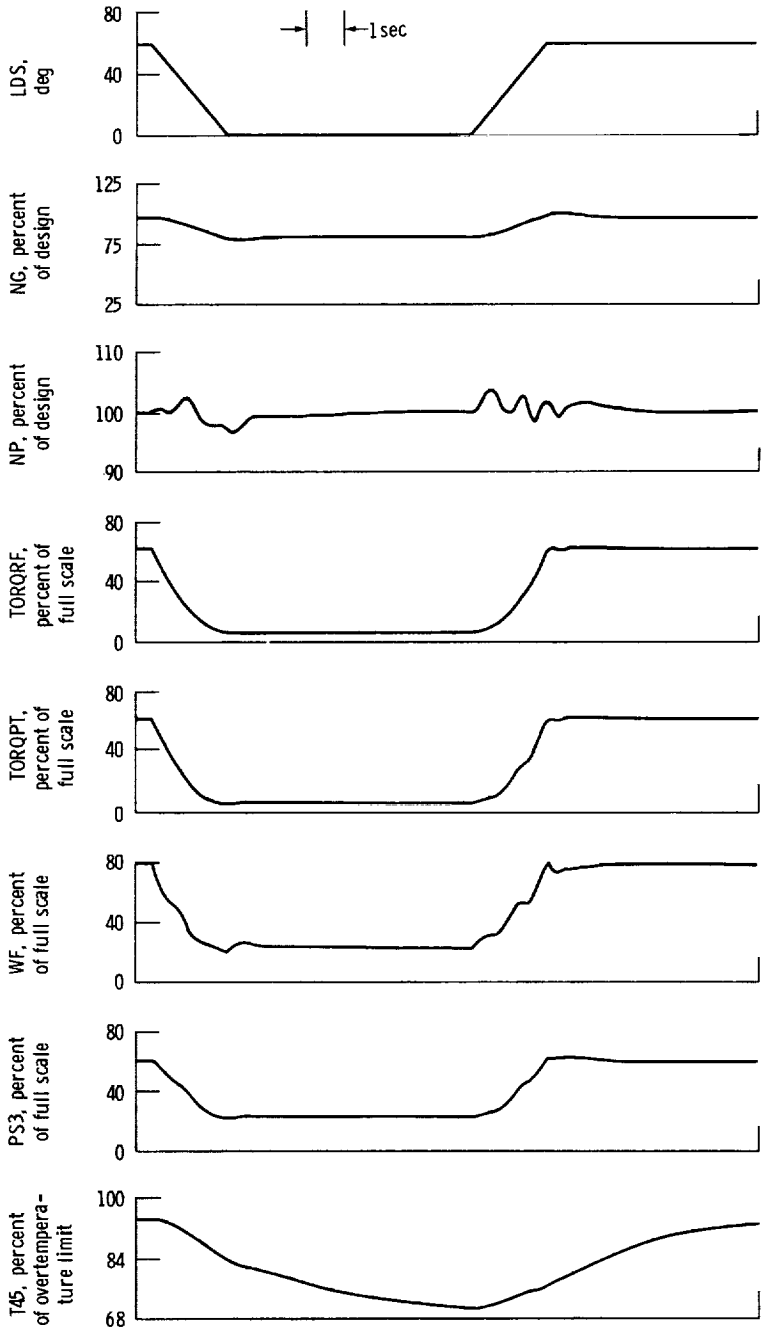

Figure 4. - Hybrid control and engine simulation transient.

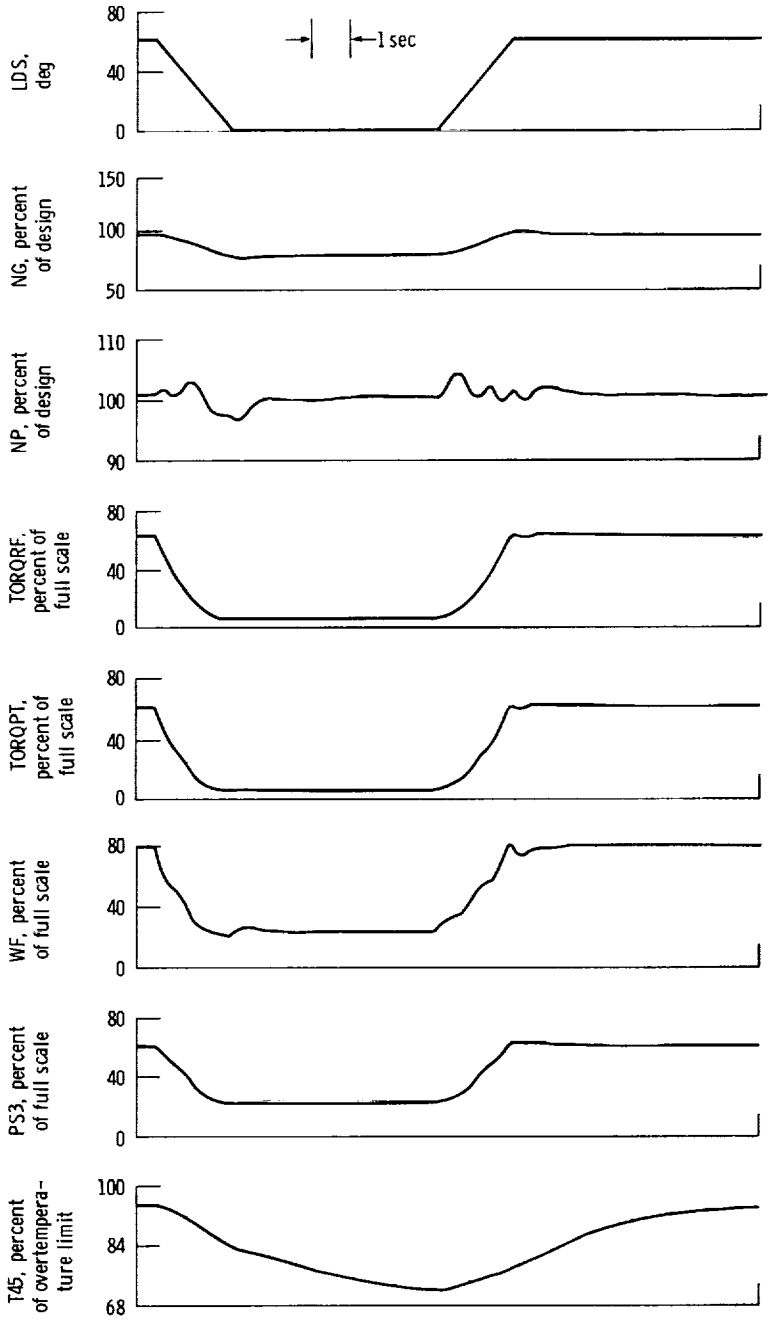

Figure 5. - Digital control module and engine simulation transient.

1. Report No.	2. Government Accession No.	3. Recipient's Catalog No.
NASA TM-83579		

4. Title and Subtitle	5. Report Date
Real-Time Hybrid Computer Simulation of a Small Turboshaft Engine and Control System	February 1984
	6. Performing Organization Code: 505-34-02
7. Author(s): Clint E. Hart and Leon M. Wenzel	8. Performing Organization Report No.: E-1968
	10. Work Unit No.
9. Performing Organization Name and Address: National Aeronautics and Space Administration, Lewis Research Center, Cleveland, Ohio 44135	11. Contract or Grant No.
	13. Type of Report and Period Covered: Technical Memorandum
12. Sponsoring Agency Name and Address: National Aeronautics and Space Administration, Washington, D.C. 20546	14. Sponsoring Agency Code

15. Supplementary Notes

16. Abstract

This report describes the development of an analytical model of a small turboshaft engine designed for helicopter propulsion systems. The model equations were implemented on a hybrid computer system to provide a real-time nonlinear simulation of the engine performance over a wide operating range. The real-time hybrid simulation of the engine was used as a test bed for evaluating a microprocessor-based digital control module. This digital control module was developed as part of an advanced rotorcraft control program that has the long-term goal of rotorcraft flight and propulsion control integration. After tests with the hybrid engine simulation the digital control module was used to control a real engine in an experimental program. A hybrid simulation of the engine's electrical-hydromechanical control system was also developed. This provided a convenient way of varying the fuel flow and torque load inputs to the hybrid engine simulation for simulating transient operation. A comparison of steady-state data obtained from the simulation and the experimental tests is presented that validates the simulation results. Analytical model equations, analog computer diagrams, and a digital computer flow chart are given in the appendixes.

17. Key Words (Suggested by Author(s))	18. Distribution Statement
Simulation; Hybrid computer; Turboshaft engine; Controls	Unclassified - unlimited STAR Category 07

19. Security Classif. (of this report)	20. Security Classif. (of this page)	21. No. of pages	22. Price*
Unclassified	Unclassified		

*For sale by the National Technical Information Service, Springfield, Virginia 22161